coatings

MDPI

Article

Microstructure, Mechanical, and Tribological Properties of Mo_2N/Ag-SiN_x Nanomultilayers with Varying Modulation Periods

Jing Luan [1,2], Lei Wang [1], Songtao Dong [1], Fábio Ferreira [2], Filipe Fernandes [2,3], Changpan Mo [4], Albano Cavaleiro [2] and Hongbo Ju [1,2,5,*]

1 School of Materials Science and Engineering, Jiangsu University of Science and Technology, Mengxi Road 2, Zhenjiang 212003, China; wangl_ray@just.edu.cn (L.W.); stdong@just.edu.cn (S.D.)
2 Centre for Mechanical Engineering, Materials and Processes, Advanced Production and Intelligent Systems, Department of Mechanical Engineering, University of Coimbra, Rua Luís Reis Santos, 3030-788 Coimbra, Portugal; fabio.ferreira@dem.uc.pt (F.F.); fid@isep.ipp.pt (F.F.); albano.cavaleiro@dem.uc.pt (A.C.)
3 Centre for Research & Development in Mechanical Engineering, ISEP-Polytechnic of Porto, Rua Dr. António Bernardino de Almeida, 4249-015 Porto, Portugal
4 COOEC-Fluor Heavy Industries Co., Ltd., No. 99, Pinggang Road, Gaolan Port Economic Zone, Jinwan District, Zhuhai 519000, China; changpan.mo@cooecfluor.com
5 TINT—Laboratory for Tribology and Interface Nanotechnology, Faculty of Mechanical Engineering, University of Ljubljana, Aškerčeva 6, 1000 Ljubljana, Slovenia
* Correspondence: hbju@just.edu.cn or hju@uc.pt

Abstract

The multilayered Mo_2N/Ag-SiN_x self-lubricant films were designed and deposited using a DC (Direct Current) magnetron sputtering system under mixed gas atmosphere of N_2 and Ar. The modulation ratio (thickness ratio of Mo_2N to Ag-SiN_x) was fixed at 2:1, while the modulation periods (thickness of Mo_2N and its adjacent Ag-SiN_x layer) were set at 20, 40, and 60 nm. The results indicated that all multilayer films, regardless of modulation period, exhibited a combination of face-centered cubic (fcc) and amorphous phases. Specifically, fcc-Mo_2N was detected in the Mo_2N layers, while fcc-Ag and amorphous SiN_x co-existed in the Ag-SiN_x layers. The multilayered architecture induced residual stress and interface strengthening, resulting in hardness values exceeding 21 GPa for all films. Compared to Mo_2N and Ag-SiN_x monolayer films, the multilayer structure significantly enhanced tribological properties at room temperature, particularly in terms of wear resistance. The Mo_2N/Ag-SiN_x multilayer films exhibit ~25% lower friction than Ag-SiN_x, ~3% lower than Mo_2N, and achieve remarkable wear rate reductions of ~71% and ~85% compared to Ag-SiN_x and Mo_2N, respectively, demonstrating superior tribological performance. The synergistic effects of both modulation layers and relative high hardness were key factors contributing to the enhanced tribological behavior.

Keywords: magnetron sputtering; Mo_2N/Ag-SiN_x multilayered films; modulation periods; tribological properties

Academic Editor: Philipp Vladimirovich Kiryukhantsev-Korneev

Received: 8 August 2025
Revised: 5 September 2025
Accepted: 9 September 2025
Published: 15 September 2025

Citation: Luan, J.; Wang, L.; Dong, S.; Ferreira, F.; Fernandes, F.; Mo, C.; Cavaleiro, A.; Ju, H. Microstructure, Mechanical, and Tribological Properties of Mo_2N/Ag-SiN_x Nanomultilayers with Varying Modulation Periods. *Coatings* **2025**, *15*, 1080. https://doi.org/10.3390/coatings15091080

1. Introduction

With the continual rise in global energy consumption, industries are placing greater emphasis on sustained advancements in cost reduction, quality improvement, and efficiency enhancement [1,2]. Friction and wear present a growing global challenge in mechanics, leading to massive energy waste and the frequent failure of critical components [3–5], and

thereby improving the surface tribological properties of complex moving and machining components has become essential [6–8]. This advancement offers a viable alternative to traditional lubrication while simultaneously enhancing equipment performance and extending operational lifespan [9–11].

As a foundational surface engineering strategy, thin-film technology provides a promising pathway to enhance the tribological performance of critical mechanical components. By optimizing film composition, structure, and deposition parameters, it enables tailored solutions for reducing friction and improving wear resistance in demanding environments [12]. Owing to their environmental sustainability, high efficiency, and economic viability, hard films fabricated via magnetron sputtering have emerged as leading materials in the contemporary hard film market [13–16]. Among these materials, molybdenum nitride (Mo_2N)-based films stand out due to their excellent mechanical and chemical stability [17–21]. These films can remarkably form self-lubricating, layered oxides in situ during friction, making them valuable for industrial applications in tools and molds [22,23]. To further enhance the friction and wear resistance, these films commonly incorporate soft metals like copper (Cu) and silver (Ag) [24–27]. These elements facilitate the in situ formation of bimetallic oxide friction layers during room- and high-temperature sliding, significantly enhancing self-lubrication across a wide temperature range [28]. Previous studies, such as those by W. Gulbinski et al., demonstrated that in magnetron-sputtered Mo_2N-Ag composites, a Ag content above 15 at.% promotes the in situ formation of $Ag_2Mo_4O_{13}$. This bimetallic oxide acts as a solid lubricant, significantly improving the tribological performance by lowering the friction coefficient [29]. The friction and wear behavior of MoN-Ag films was further investigated by X. Xu et al., who reported a low average friction coefficient of 0.27 at 700 °C, resulting from the in situ generation of lubricious tribofilms [30].

Although Mo_2N-based films incorporating soft metals exhibit excellent self-lubricating performance across a wide temperature range, they are constrained by two major limitations: (i) degradation of mechanical properties (hardness, adhesion) under extreme conditions, and (ii) uncontrolled formation of layered tribo-phases that compromise wear resistance [31]. To solve this challenge, the amorphous hard phase/layer was incorporated into the self-lubricant matrix to avoid the excessive formation of the layered tribo-phases as well as the drop in hardness [32–36]. For instance, amorphous SiN_x is added to the Mo_2N-Ag composite film, and the alloy composition is optimized to produce a material exhibiting the classic "amorphous-encapsulated nanocrystal" microstructure. This design enables the controlled release of soft metals while providing protection for the Mo_2N matrix [37]. In addition, the multilayered structural design can also achieve the protection of the lubricating components through the alternating deposition of amorphous SiN_x barrier layer and Mo_2N-Ag lubricating layer, so that the film has a certain continuous lubricant ability under room-temperature–high-temperature cycle environment [38]. Nevertheless, the previously mentioned film design fails to mitigate the decline in mechanical properties arising from the incorporation of soft metals, as these metals do not dissolve within the nitride lattice. Therefore, the addition of sufficient soft metals can improve the self-lubricant properties of the film, but it will have a significant attenuation effect on the mechanical properties.

This study aims to solve the above problems through film structure design and composition optimization. Therefore, on the basis of the previous research conclusions, this paper selects the optimized Mo_2N film [31] as a modulation layer and the optimized Ag-SiN_x film [39] as another modulation layer. By optimizing the modulation period of the multilayered film, the synergism effect of both modulation layers is guaranteed to meet the lubrication performance requirements, and the multilayer film interface effect induced by the alternating deposition of the modulation layers is used to offset the mechanical performance attenuation caused by the addition of soft metals. This paper investigates a

series of Mo_2N/Ag-SiN_x multilayer films with a fixed modulation ratio of 2:1 and varying modulation periods. The films were synthesized via magnetron sputtering by alternately depositing Mo_2N and Ag-SiN_x layers. Their microstructure, mechanical properties, and tribological performance were characterized using X-ray diffraction (XRD), transmission electron microscopy (TEM), nanoindentation, and a friction and wear test.

2. Experimental Information

2.1. Sample Preparation

The magnetron sputtering system was used to deposit the Mo_2N/Ag-SiN_x multilayer films. There are three rectangular cathodes assembled on the chamber wall. The angle between two adjacent cathodes is 90°. Mo target, Si target, and Ag target with a purity of 99.9% are fixed on three independent cathodes, respectively. The size of the cathode is 380 × 175 mm. The cathodes are connected to a DC power supply. The size of the substrate is 60 × 60 × 4 mm. Polished WC (Tungsten Carbide, adhesion of all deposited specimens was around 18 N) and Si (100) wafers were used as substrates in the depositions. Before depositions, the substrates were ultrasonically cleaned in alcohol for 15 min and acetone for 15 min. WC substrates were used for mechanical and tribological properties evaluation (hardness, elastic modulus, and tribological assessment), whilst Si substrates were used for XRD and TEM analyses. The minimum distance between the targets and substrates was set to 55 mm. Prior to the depositions, the chamber was vacuumed down below 1.0×10^{-4} Pa. A Mo adhesion layer with thickness 150 nm was firstly deposited under Ar flow of 50 sccm, in order to improve the adhesion of the films to the substrate. After that, the multilayer structure was deposited by moving the shutter in the front of Si and Ag target for the Mo_2N layer, in an alternating way for the Ag-SiN_x layer, in the presence of a N_2 atmosphere. The multilayered structure was grown by applying a power 1.5, 0.6, and 0.2 kW at the Mo, Si, and Ag targets, respectively, in all the depositions. The Ar and N_2 partial pressures were 0.38 and 0.12 Pa, corresponding to a total working pressure of 0.5 Pa. The gas mass flow during the deposition was kept at 70 sccm. Films with different modulation periods (the thickness of the layer of Mo_2N and its adjacent Ag-SiN_x) of 20, 40, and 60 nm, with a fixed modulation ratio (ratio of thickness of Mo_2N to Ag-SiN_x) of 2:1, were produced by controlling the sputtering time from the Mo, Ag, and Si targets. The deposition rate of the Mo_2N and Ag-SiN_x layers was 0.6 and 0.4 nm/s, respectively. The deposition time of each modulation layer was calculated by the designed modulation periods. The substrate one-fold rotation speed was kept at 10 rpm during the deposition. The total thickness of the as-deposited film was kept at approximately 2 μm. The depositions were performed at room temperature and were made with the grounded substrate.

2.2. Microstructure and Surface Observation

The crystal structure of the films was characterized by X-ray diffraction using a Shimazu-6000 (Shimadzu, Kyoto, Japan) with Cu Kα radiation at a pass energy of 160 eV. Measurements were taken over a 2θ range of 20–80°, with a step size of 4°/min. The elemental chemical composition of the reference Mo_2N and Ag-SiN_x monolayers was analyzed using an energy-dispersive spectrometer (EDS, Oxford Instruments, Abingdon, UK). The microstructure was examined using a JEOL JEM-2100F transmission electron microscope (JEOL, Tokyo, Japan) operating at 200 kV. TEM specimens were first mechanically polished on both sides with diamond sandpaper until their thickness was reduced to approximately 0.1 mm. A molybdenum ring was then attached to the sample surface to provide support, and final thinning to electron transparency was achieved using an ion beam milling system (Gatan 691, Gatan, Pleasanton, CA, USA).

2.3. Mechanical Properties

Hardness and elastic modulus of the films were investigated using the CPX + NHT2 + MST nano-indentation system (Anton Paar, Baden, Switzerland), applying a constant load of 3 mN and a holding time of 10 s. The system was equipped by a Berkovich diamond indenter. The loading and unloading rates were set at 0.1 mN/s. Measurements were performed on two distinct areas of each specimen, with fifteen measurements per area. The film curvature radii were measured using the profilometer (DEKTAK-XT, Bruker, Ettlingen, Germany), and then the residual stress of the films with different silver content was calculated based on Stoney's equation [40]. The Stoney equation assumes a thin, uniform coating and an elastically deforming substrate, which may overlook local stresses or multilayer effects. Uncertainty also arises from variations in coating properties such as elastic modulus and Poisson's ratio. More accurate residual stress evaluation could be obtained with techniques like $\sin^2 \psi$ XRD or complementary wafer curvature analysis, which were beyond the scope of this study but remain important for future work. A mask was used to produce a step, and the film thickness was also measured using the profilometer. An average was calculated from the total of thirty measurements to ensure accuracy and consistency.

2.4. Tribological Properties

The friction and wear resistance properties at room temperature were evaluated using a ball-on-disk tribometer (UMT, UMT-2, CETR, Campbell, CA, USA). The tribo-tests were conducted at a rotational speed of 50 rpm for 30 min, under a normal load of 5 N, using an alumina ball (9.5 mm diameter) as the counterpart. The relative humidity during the testing was approximately 30%. The average coefficient of friction was calculated from the steady-state portion of the friction curve. Raman spectroscopy was performed using an Ar^+ laser excitation source in a backscattering optical configuration. Wear track was measured using 2D profilometry (BRUKER, Dektak-XT, Germany) four times from different zones of the wear track, and wear rates were calculated using the formula in Ref. [41] (Table 1); the formula is as follows:

$$W_s = \frac{C \times S}{F \times L}$$

where W_s—wear rate ($mm^3 \cdot N^{-1} \cdot mm^{-1}$)

C—wear mark perimeter (mm);
S—average area of wear track (mm^2);
F—normal load (N);
L—sliding distance (mm).

Table 1. Table with summary of experimental parameters.

Parameter Category	Experimental Parameters	Method/Value
Substrate	Material and Size	WC (60 × 60 × 4 mm), Si (100)
Deposition Environment	Base Pressure	<1.0×10^{-4} Pa
Layer Structure	Adhesion Layer	Mo (150 nm)
Deposition Process	Modulation Period (Λ)	20, 40, 60 nm (Mo_2N/Ag-SiN_x)
	Total Film Thickness	~2 μm
	Target Power (Mo/Ag-Si)	1.5 kW/0.2 kW
	Sputtering Gas Flow (Ar/N_2)	70 sccm (Ar: 0.38 Pa, N_2: 0.12 Pa)
	Deposition Rate (Mo_2N/Ag-SiN_x)	0.6 nm/s/0.4 nm/s
	Substrate Rotation Speed	10 rpm

Table 1. *Cont.*

Parameter Category	Experimental Parameters	Method/Value
Characterization	X-ray Diffraction (XRD) Transmission Electron Microscopy (TEM)	Shimadzu-6000 JEOL JEM-2100F
Mechanical Testing	Nanoindentation	3 mN load, Berkovich tip
Tribological Testing	Ball-on-disk Test	5 N load, Al_2O_3 ball (9.5 mm), 50 rpm

3. Results and Discussion

3.1. Microstructure of the Multilayer Films

The elemental composition of the corresponding monolayered Mo_2N and Ag–SiN_x films was determined by energy-dispersive X-ray spectroscopy (EDS). Mo_2N reference films: Mo (58.2 at.%), N (40.7 at.%), and O (1.1 at.%). Ag–SiN_x films: Ag (16.4 at.%), Si (39.6 at.%), N (41.3 at.%), and O (2.7 at.%). In our previous study, the monolithic SiN_x layer contained 45.3 at.% Si, 50.5 at.% N, and 4.2 at.% O, so these compositional results are in good agreement with our previously optimized system [38].

Figure 1 shows the XRD pattern of Mo_2N, Ag-SiN_x reference films, and Mo_2N/Ag-SiN_x multilayer films with different modulation periods (Λ). As can be seen from this figure, the XRD pattern of the binary Mo_2N multilayer film shows six diffraction peaks, located at 36.4, 42.4, 61.8, 66.8, 73.2, and 77.4° in sequence. Except for the diffraction peak near 69° coming from the substrate of silicon wafer, the remaining ones all come from the as-deposited film. According to JCPDF # 25-1366, these diffraction peaks correspond to fcc-Mo_2N (111), (200), (220), (311), and (222) from low to high angle. But four diffraction peaks appeared in its enlarged pattern in Figure 1b, among which the diffraction peak near 69° comes from the silicon wafer substrate. According to PDF # 89-3722, the three diffraction peaks at 39, 45, and 65° are all from the fcc-Ag phase, and the corresponding crystal planes are (111), (200), and (220), respectively. No diffraction peaks of silicon nitride and other silicon compounds were found in the pattern. As a matter of fact, the result from the XRD pattern is followed by the ones in our previously published paper [38]. Through the study of the microstructure of this kind of film, it was found that the film is composed of two phases, fcc-Ag and amorphous a-SiN_x, in which Ag nanocrystals are dispersed in the amorphous matrix [38]. For Mo_2N-Ag-SiN_x multilayer films with different Λ, six diffraction peaks appeared in their XRD pattern, which are located in 36.4, 42.4, 61.8, 66.8, 73.2, and 77.4° in sequence. With the exception of the diffraction peak near 69°, the remaining five peaks can be attributed to the fcc phases of Mo_2N and Ag. The explanations for this situation are as follows: (i) the multilayer film is obtained by alternating deposition of two modulation layers of Mo_2N and Ag-SiN_x, so the crystal planes parallel to the sample surface from the two modulation layers contribute to the overall XRD pattern of the multilayer film; (ii) the diffraction peaks of fcc-Mo_2N and fcc-Ag with the same crystal plane index are very close, so the diffraction peaks of the two phases with the same crystal plane index in the multilayer film may overlap with each other, and there is no obvious diffraction peak separation. In addition, compared with the Mo_2N and Ag-SiN_x monolayer films, the diffraction peaks of the Mo_2N/Ag-SiN_x multilayer film are slightly offset to the low-angle direction. As for the magnetron-sputtered nitride-based films, such as TiN [42], the residual stress normally increased by the decrease in the thickness. During the deposition of multilayer films, due to the alternating deposition of Mo_2N and Ag-SiN_x modulation layers, the thickness of the two modulation layers ranges from a few nanometers to tens of nano-meters. Therefore, the residual stress of the two modulation layers is higher than that of the single-layer film. Then it results in the diffraction peak of the multilayer film shifting toward the low-angle direction. The peak shifts observed were

minimal and within the expected experimental error range; therefore, the stress values were potentially unreliable without more advanced analysis.

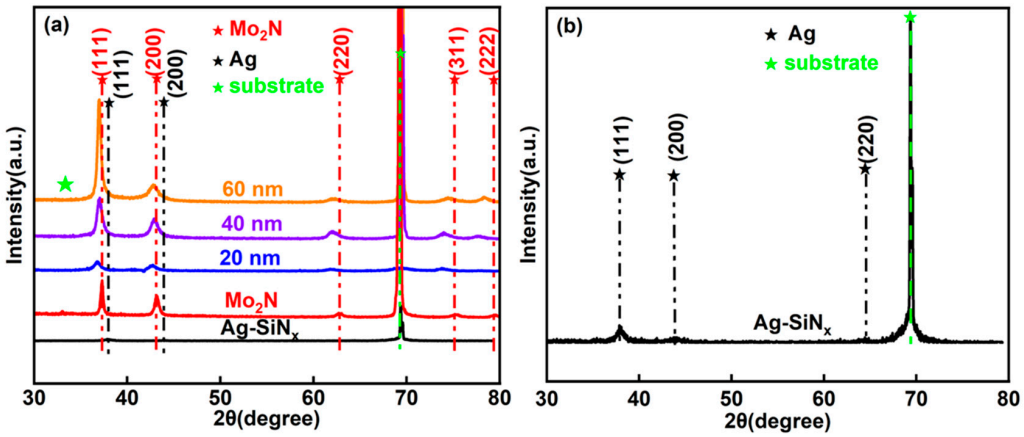

Figure 1. (**a**) XRD patterns of the Mo_2N, Ag-SiN_x reference films, and the Mo_2N/Ag-SiN_x multilayered films with the modulation period of 20, 40, and 60 nm; (**b**) the enlarged XRD pattern of the Ag-SiN_x reference film.

Moreover, the increase in diffraction peak intensity (particularly for the (111) peak) with modulation period (Λ) suggests that a larger period improves the alignment of diffraction planes parallel to the specimen surface.

Figure 2 shows a cross-sectional TEM photo of a Mo_2N/Ag-SiN_x multilayer film with a modulation period of 20 nm. A dense cross-sectional microstructure was observed. Figure 2a shows that the film is composed of two modulation layers deposited alternately, in which the brighter modulation layer is the Ag-SiN_x layer, and the darker is the Mo_2N layer. Its enlarged image is shown in (b), and the interface between the modulation layers is clear. Within the Ag-SiN_x layer, subtle dark spots (as shown in the marked zone in Figure 2b) are dispersed amidst the brighter regions. Based on the synthesis parameters and in agreement with previous studies [43], these particles were consistent with Ag nanoparticles. The thickness of the Ag-SiN_x layer is about 7 nm, the thickness of the Mo_2N layer is about 13 nm, the thickness ratio of the two layers is about 1:2, and the total thickness of the two layers is about 20 nm, which is consistent with the results of the film design.

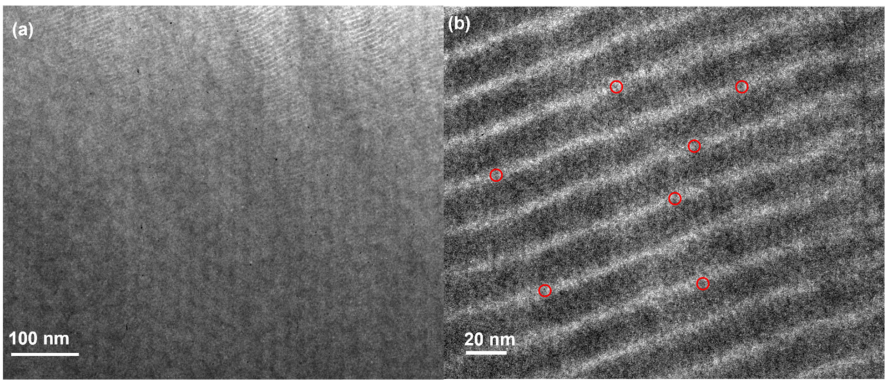

Figure 2. The cross-sectional TEM image (**a**) of the Mo_2N/Ag-SiN_x multilayered film with a modulation period of 20 nm, and its magnified view (**b**).

Based on the above experimental results, for the Mo_2N/Ag-SiN_x multilayer films with a modulation ratio of 1:2 and different Λ, the interface between the modulation layers is clear, the Mo_2N layer has an fcc structure and is a Mo_2N phase, while the Ag-SiN_x layer has two phases coexisting, consisting of fcc-Ag and amorphous SiN_x.

3.2. Mechanical Properties of the Multilayer Films

Figure 3 illustrates the indentation load–displacement curves and hardness of the Mo_2N, Ag-SiN_x reference films, and the Mo_2N/Ag-SiN_x multilayered films with the Λ of 20, 40, and 60 nm. As shown in Figure 3a, the maximum indentation depth for all specimens was below 100 nm. Since this depth is less than 10% of the total film thickness (~2000 nm), substrate effects can be considered negligible. The hardness of monolayered Mo_2N and Ag-SiN_x film is approximately 28 and 7 GPa, respectively. The hardness of multilayered films, regardless of Λ, are all higher than the calculated one. The calculated one refers to the hardness value estimated using the rule of mixtures. Additionally, the hardness decreases slightly with the increase of Λ.

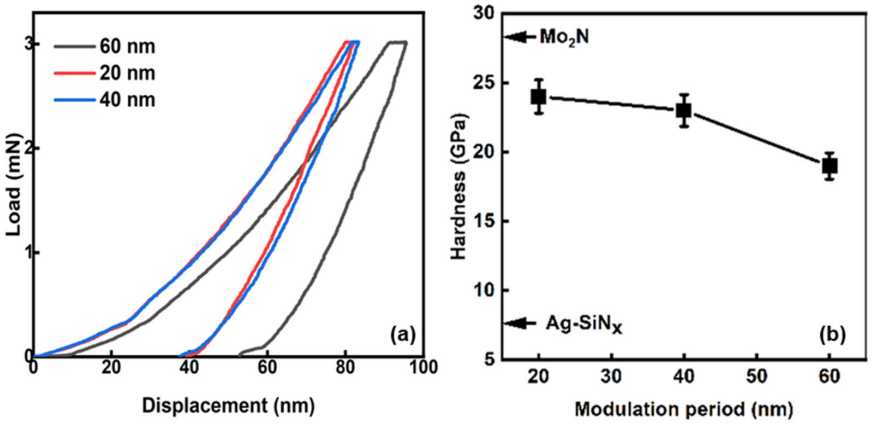

Figure 3. The indentation load–displacement curve (**a**), and hardness (**b**) of the Mo_2N, Ag-SiN_x reference films, and the Mo_2N/Ag-SiN_x multilayered films with the modulation period of 20, 40, and 60 nm.

Although coherent strengthening is a primary mechanism for enhancing the mechanical properties of nano-multilayer films, its effect is highly dependent on the modulation period (Λ) [44]. The observed strengthening is likely the result of a combination of residual stress, interface barriers, dislocation blocking by the amorphous phase, and the contribution of nanocrystalline Ag, rather than being dominated by a single factor. For instance, inserting Ag layer with a thickness of around 4 nm into the TiN matrix could enhance the hardness, but this kind of enhancement totally disappeared once the size of Ag was larger than 4 nm, due to the disappearance of the coherent structure of Ag epitaxy growth with the TiN template [44]. Additionally, the SiN_x phase was also reported to possibly grow epitaxially on the nitride-based template, such as Mo_2N, but its critical thickness was calculated to be less than 1 nm [43]. Since the designed Ag–SiN_x layer thicknesses in this work all exceed the critical thickness required for forming a coherent interface, the hardness of the multilayers typically follows the rule-of-mixtures model [43], whereby the overall hardness is primarily governed by the intrinsic hardness of each constituent layer and their respective volume fractions. The critical thickness for maintaining coherent interfaces in Ag/SiN_x multilayers has been reported to lie in the range of approximately 2–5 nm, beyond which lattice mismatch and strain accumulation lead to the formation of misfit dislocations and semi-coherent or incoherent interfaces, thus invalidating coherency-based strengthening mechanisms [39]. Therefore, the calculated hardness of the multilayered film, regardless of the modulation periods, is stable at 21 GPa. However, the actual measured hardness is inconsistent with its value: (i) the actual measured hardness value of the multilayer film is significantly higher than the calculated result; (ii) The hardness of the multilayer film gradually decreases with the increase of Λ. The actual measured hardness

of Mo_2N/Ag-SiN_x multilayered films with the Λ of 20, 40, and 60 nm is 25 GPa, 23 GPa, and 21 GPa, respectively.

For the phenomenon of measured hardness higher than the calculated ones, the following explanations can be given: (i) Residual stress. The residual stress of the multilayered film, calculated using the Stoney formula [45], is approximately −1.7 GPa (the negative value indicates compressive stress). This stress level appears to be relatively unaffected by the modulation period (Λ). For comparison, the residual stresses of the monolayer Mo_2N and Ag–SiN_x films were also measured, yielding values of approximately −1.5 GPa and −0.4 GPa, respectively. These values are slightly higher than those reported in previous studies involving RF magnetron sputtering [31,38], which may be attributed to the higher sputtering power applied in the present work. Notably, all multilayered films possess higher residual stress than their monolayer counterparts, likely due to the coherency stresses and interfacial constraints arising from the layered structure [46]. This observation, which aligns with the noted diffraction peak shifts, points to increased lattice distortion or interfacial strain in the multilayered architecture. (ii) Interface effect. The alternating deposition of the two modulation layers results in a clear interface between the adjacent modulation layers, which hinders the slip of dislocations and ultimately leads to a hardness that is slightly higher than the value calculated by the mixed rule.

The observed decrease in measured hardness with increasing modulation period (Λ) can be attributed to two main factors: (i) The interface strengthening effect, as the hardness measurements were performed using a nanoindenter with a constant load of 3 mN. As Λ increases, the number of interfaces within the indentation depth decreases. Since interfaces can act as effective barriers to dislocation motion, a higher interface density enhances hardness, analogous to the Hall–Petch effect observed in grain-refined materials, where smaller grain (or layer) sizes lead to increased resistance to plastic deformation [47]. Although the mentioned multilayered system does not show a perfect Hall–Petch-type linearity, the observed trend aligns qualitatively with interface-controlled strengthening models commonly seen in nanoscale multilayers. (ii) Influence of top-layer thickness and heterogeneity. Under constant load conditions, the maximum indentation depth remained below 100 nm. In our multilayer structure, the top layer is Ag–SiN_x, which has significantly lower hardness (~7 GPa) and elastic modulus (~153 GPa) compared to Mo_2N (~28 GPa) and elastic modulus (~160 GPa). With increasing Λ, the Ag–SiN_x layer becomes thicker, reducing the relative contribution of the harder Mo_2N layers to the measured response. This geometric effect, combined with the reduced interface density, contributes to the overall decrease in apparent hardness. Although a direct Hall–Petch-type (i.e., hardness $\propto 1/\sqrt{\Lambda}$) or linear interface-spacing-based correlation is not strictly observed, the trend supports a qualitative mechanistic linkage between modulation periods. Deviation from the ideal Hall–Petch relationship may arise from the amorphous Ag–SiN_x layer, incoherent interfaces, and effects of interlayer mixing or interface roughness.

3.3. Tribological Properties of the Multilayer Films

Figure 4 shows the average friction coefficient and wear rate of Mo_2N/Ag-SiN_x multilayer films at room temperature with different Λ. As shown in Figure 4a, the average friction coefficients of Mo_2N and Ag-SiN_x monolayer films are 0.31 and 0.40, respectively. The average friction coefficient of Mo_2N/Ag-SiN_x multilayer films is slightly lower than that of the two films, but its value is not greatly affected by Λ and is roughly stable at around 0.30. Specifically, the multilayer films exhibit an average friction coefficient of 0.30, which is approximately 25% lower than that of the Ag-SiN_x monolayered film (0.40) and 3.2% lower than that of the Mo_2N monolayered film (0.31). The wear rates of the Mo_2N and Ag-SiN_x monolayered films are around 6.3×10^{-6} mm^3/N.mm, and 3.2×10^{-6} mm^3/N·mm,

respectively. The wear rate of the multilayer film deposited alternately by Mo_2N and Ag-SiN_x is significantly lower than that of the above two monolayer films. Like the average friction coefficient of the multilayer film, its value is not greatly affected by Λ. The wear rate of Mo_2N/Ag-SiN_x multilayer film is roughly stable at 9.2 × 10^{-7} mm^3/N·mm.

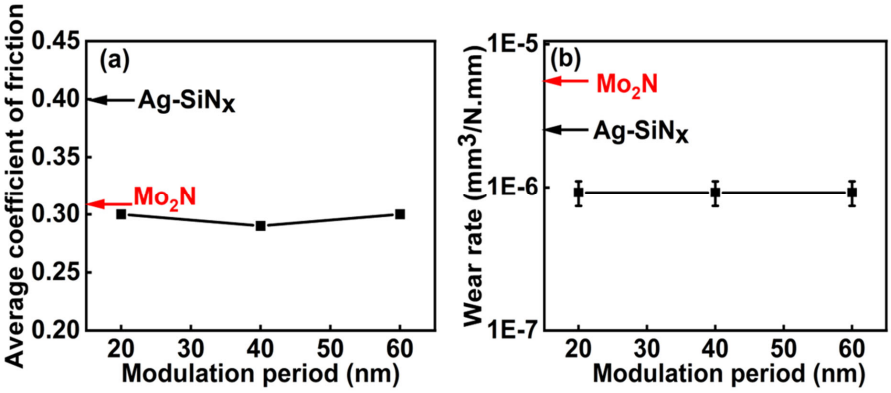

Figure 4. Room temperature average coefficient of friction (**a**) and wear rate (**b**) of the Mo_2N/Ag-SiN_x multilayered films with the modulation period of 20, 40, and 60 nm.

During the friction experiment, the two modulated layers can react with oxygen and water vapor in the environment and adsorbed substances on the surface of the film under the action of the grinding pair to generate a complex friction chemical reaction between the two modulated layers and the friction phase. Studies have shown that even at room temperature, the Mo_2N film can generate the friction phase MoO_3 in situ under the action of the ceramic-based grinding pair [31]. This friction phase has a layered structure, is easy to slip under the action of shear force, and has a self-lubricating effect [43]. In addition, some studies have shown that for Mo_2N films containing Ag, self-lubricant bimetallic oxides can be generated under room-temperature friction conditions [29,37]. More importantly, under the same friction experimental environment as this article, we characterized the presence of $Ag_2Mo_4O_{13}$ [48] in the wear scar of the Mo_2N film containing Ag through Raman spectroscopy.

Figure 5 illustrates the 2D morphology of the wear track from the reference monolayered film and the multilayered film at Λ 20 nm. As shown in Figure 5a, the width of the wear track from the Ag-SiN_x monolayer film exhibits the widest width, with a value of approximately 1.5 mm. The lowest hardness of the as-deposited film mainly results in it. The depth of the wear track is around 1 μm. The wear track of the monolayered Mo_2N film shows the different characteristics, compared with the SiN_x one. Figure 5b illustrates a relatively short wear track with a width of about 1.0 mm. The shortened wear track width is mainly attributed to the high hardness of the as-deposited film. However, the depth of the wear track seems to be deeper than the one from Figure 5a. The deepest value on the center of the wear track is almost touched by the total thickness of the as-deposited film. Additionally, the accumulation of the wear debris is obviously detected on both sides of the wear track. And a lot of scratches appear on the center of the wear track. The asperities on the wear track surface were first in contact with the counterpart at the beginning of the wear test, and then some of them were crushed under the load force and moved along with the counterpart. Although the self-lubricant tribo-phase of MoO_3 was widely reported to be formed by the tribo-chemical actions, even under the RT tribo-testing conditions [31,38,49], the hard wear debris still scratches the wear track surface by moving with the counterpart. Consequently, the wear debris could be continuously generated under the scratching of the remaining ones, and finally its accumulation on both sides of the wear track. As shown in Figure 5c, the wear track is shorter than that in Figure 5b, which indicates that the

alternating use of the Ag-SiN_x layer and Mo_2N layer can enhance the wear resistance. Compared with the Ag-SiN_x monolayer film, the increased hardness of the multilayered one results in the shortened width of the wear track. The disappearance of the obvious debris accumulation on both sides of the wear track is attributed to the decreased depth, compared with the Mo_2N reference one.

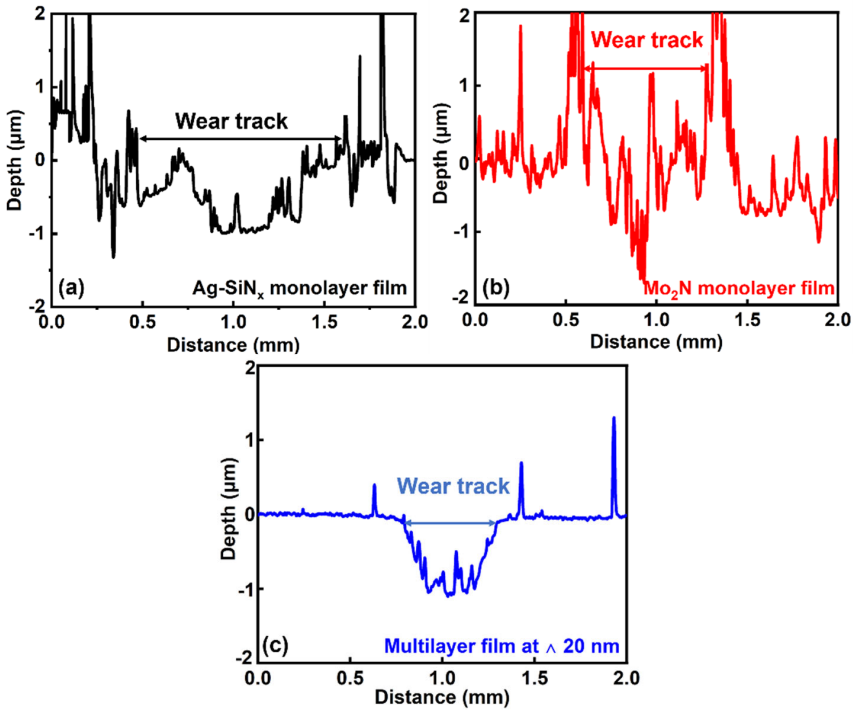

Figure 5. Two-dimensional wear track of the Ag-SiN_x (**a**), Mo_2N (**b**) monolayered film, and the multilayered film with the Λ of 20 nm (**c**).

Figure 6 shows the optical morphology and Raman spectrum of the wear track for the multilayer film with a 20 nm modulation period. As shown in Figure 6a, fine scratches are clearly observed on the wear track surface, and some regions appear significantly darker compared to the as-deposited film. During the wear test, the counterpart contacts the film surface under an applied load, resulting in material removal and the generation of wear debris. Some debris is carried away by the counterpart, while harder fragments contribute to further abrasion, forming the observed fine scratches. In addition to mechanical wear, tribo-chemical reactions also occur, even at room temperature, due to localized frictional heating. These reactions, particularly with ambient oxygen or moisture, can lead to the formation of tribo-oxides or other surface phases. The darker areas on the wear track are likely attributed to the accumulation of such tribo-phases, which alter the optical appearance of the worn surface. Figure 6b shows the Raman spectrum obtained from the wear track surface. The detected Raman peaks correspond to three distinct tribo-phases: MoO_3 [31], SiO_2 [50], and $Ag_2Mo_4O_{13}$ [51]. These findings are consistent with our previous study on Mo_2N/Ag-SiN_x multilayered films with thinner Ag-SiN_x layers [38]. Among the observed peaks, those associated with MoO_3 exhibit the highest intensity and quantity, indicating that the layered MoO_3 tribo-phase is the dominant species formed during sliding. This suggests that MoO_3 plays a crucial role in reducing friction and contributes significantly to the self-lubricating behavior of the multilayer film. The Raman spectra are used for identification rather than quantitative phase analysis, and the relative intensities should be interpreted qualitatively.

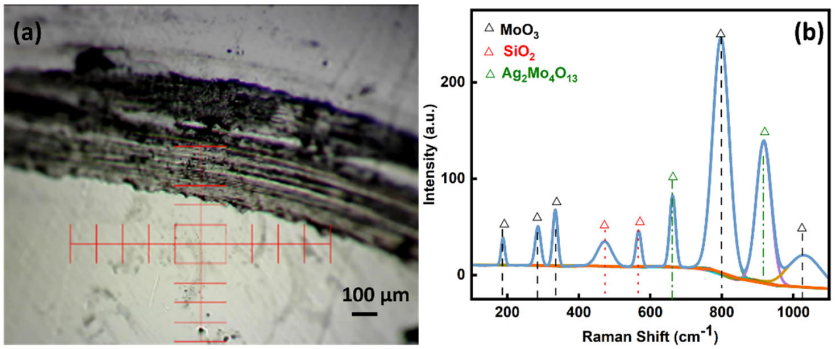

Figure 6. (**a**) The optical morphology of the wear track for the multilayer film with a 20 nm modulation period and (**b**) Raman spectrum.

In summary, the synergistic effect of the two lubricating phases yields a superior room-temperature tribological performance. The multilayer film's average friction coefficient is significantly lower than that of the Ag-SiN_x monolayer and marginally lower than that of the Mo_2N monolayer. The wear behavior of the Mo_2N/Ag–SiN_x multilayers differs markedly from that of the Mo_2N monolayer. While the monolayer exhibits continuous crack propagation and localized delamination, the multilayer architecture modifies the failure mode. The amorphous SiN_x interlayers act as effective crack-arrest and deflection barriers, while the nanocrystalline Ag phase contributes to stress relaxation within the structure. As a result, crack propagation is interrupted, and the dominant wear mechanism shifts from brittle fracture and spallation to more stable processes involving mild abrasion and plastic deformation. This demonstrates that layer modulation not only enhances hardness but also improves resistance to catastrophic failure by promoting interface-controlled crack deflection and energy dissipation.

As for the wear rate of multilayer films, a lower average friction coefficient often means that the interaction between the grinding pair and the film tends to be relaxed, which also has a certain improvement effect on wear, to a certain extent. In addition, the wear rate of the film is also affected by hardness. The film with high hardness maybe reflects its high capacity of load bearing [52–54]. Although the hardness of the multilayered film gradually decreases with the modulation period, the wear rate exhibits an independence on the hardness. The modulation ratio of multilayer films with different Λ is constant at 2:1, and the atomic percentage of each element is relatively constant (see the microstructure part). It can be considered that the friction phases during the friction process are roughly similar, and because the hardness of the multilayer film does not change much, the average friction coefficient and wear rate of the multilayer film are not greatly affected by Λ.

4. Conclusions

Self-lubricating films are crucial for engineering and environmental protection as they reduce friction without traditional lubricants; thus, enhancing their hardness and wear resistance without compromising their lubricity has become a key research goal in solid lubrication. The conclusion mainly includes the following parts:

(i) The multilayered Mo_2N/Ag–SiN_x self-lubricating films were successfully fabricated using DC magnetron sputtering with a fixed modulation ratio of 2:1. Varying the modulation period between 20, 40, and 60 nm resulted in well-defined multilayer structures, comprising fcc-Mo_2N in the Mo_2N layers and a combination of fcc-Ag and amorphous SiN_x in the Ag–SiN_x layers. The alternating deposition of these layers introduced residual compressive stress and strong interfacial bonding, which contributed to the structural stability of the films.

(ii) The multilayer architecture significantly enhanced the mechanical performance of the films. All multilayer variants exhibited hardness values exceeding 21 GPa, attributable to interface strengthening and the residual compressive stress induced by the layered structure. This represents a marked improvement over the monolayer Mo_2N and Ag–SiN_x films.

(iii) The multilayer films demonstrated superior tribological performance at room temperature compared with their monolayer counterparts, particularly in terms of wear resistance. The improvement was primarily due to the synergistic effect of the modulation layers, the relatively high hardness, and the formation of self-lubricating MoO_3 tribo-phases during sliding. These features highlight the potential of the multilayer Mo_2N/Ag–SiN_x films for industrial applications, including cutting tools and molds.

Future research will address the limitations of this study. Specifically, systematic nanoindentation across multiple regions will provide more precise elastic modulus (E) measurements. The multilayer structure will be characterized in greater detail using SEM/EDS for elemental mapping and phase contrast imaging. Finally, tribological analysis will be enhanced with complete friction coefficient curves, quantitative Raman spectroscopy of wear tracks, and comprehensive SEM to elucidate wear mechanisms.

Author Contributions: Conceptualization, S.D.; Methodology, S.D., F.F. (Fábio Ferreira), F.F. (Filipe Fernandes) and H.J.; Software, L.W.; Validation, C.M.; Formal analysis, L.W. and F.F. (Fábio Ferreira); Investigation, J.L., L.W., F.F. (Fábio Ferreira) and C.M.; Resources, L.W., F.F. (Fábio Ferreira), C.M. and A.C.; Data curation, S.D.; Writing—original draft, J.L. and H.J.; Writing—review & editing, F.F. (Filipe Fernandes) and H.J.; Visualization, S.D.; Supervision, F.F. (Filipe Fernandes) and A.C.; Project administration, A.C.; Funding acquisition, H.J. All authors have read and agreed to the published version of the manuscript.

Funding: Supported by the projects granted by the National Natural Science Foundation of China with the number of 52171071, national funds through FCT of Portugal—Fundação para a Ciência e a Tecnologia, under a scientific contract of 2021.04115.CEECIND, 2023.06224.CEECIND, and under projects UID/00285-Centre for Mechanical Engineering, Materials and Processes and LA/P/0112/2020, the Slovenian Research Agency ARIS under the Research Core Funding Programme No. P2-0231 and the Marie Skłodowska-Curie Actions (MSCA) with the number of MSCA-COFUND-5100-237/2023-9.

Data Availability Statement: The original contributions presented in this study are included in the article. Further inquiries can be directed to the corresponding author.

Conflicts of Interest: Author Changpan Mo was employed by the company COOEC-Fluor Heavy Industries Co., Ltd. The remaining authors declare that the research was conducted in the absence of any commercial or financial relationships that could be construed as a potential conflict of interest.

References

1. Swain, B.; Yang-Wallentin, R. Achieving sustainable development goals: Predicaments and strategies. *Int. J. Sustain. Dev. World Ecol.* **2020**, *27*, 96–106. [CrossRef]
2. Holmberg, K.; Erdemir, A. Influence of tribology on global energy consumption, costs and emissions. *Friction* **2017**, *5*, 263–284. [CrossRef]
3. Sun, Z.; Wang, Q.; Ning, X.; Fan, J.; Li, L. Microstructure and thermal cycling behavior of Mo $(Si, Al)_2$ dispersed GYYSZ multilayer composite coatings on molybdenum substrate under extreme environmental conditions. *Surf. Coat. Technol.* **2025**, *512*, 132400. [CrossRef]
4. Li, Y.; Xiao, Y.; Yu, L.; Ji, K.; Li, D. A review on the tooling technologies for composites manufacturing of aerospace structures: Materials, structures and processes. *Compos. Part A Appl. Sci. Manuf.* **2022**, *154*, 106762. [CrossRef]
5. Sarfraz, M.S.; Hong, H.; Kim, S.S. Recent developments in the manufacturing technologies of composite components and their cost-effectiveness in the automotive industry: A review study. *Compos. Struct.* **2021**, *266*, 113864. [CrossRef]

6. Hegab, H.; Kishawy, H.A.; Darras, B. Sustainable cooling and lubrication strategies in machining processes: A comparative study. *Procedia Manuf.* **2019**, *33*, 786–793. [CrossRef]
7. Wu, T.; Blawert, C.; Serdechnova, M.; Karlova, P.; Dovzhenko, G.; Wieland, D.C.F.; Stojadinovic, S.; Vasilic, R.; Wang, L.; Wang, C.; et al. Role of phosphate, silicate and aluminate in the electrolytes on PEO coating formation and properties of coated Ti6Al4V alloy. *Appl. Surf. Sci.* **2022**, *595*, 153523. [CrossRef]
8. Studeny, Z.; Krbata, M.; Dobrocky, D.; Eckert, M.; Ciger, R.; Kohutiar, M.; Mikus, P. Analysis of Tribological Properties of Powdered Tool Steel M390 and M398 in Contact with Al_2O_3. *Materials* **2022**, *15*, 7562. [CrossRef]
9. Sartori, S.; Ghiotti, A.; Bruschi, S. Hybrid lubricating/cooling strategies to reduce the tool wear in finishing turning of difficult-to-cut alloys. *Wear* **2017**, *376–377*, 107–114. [CrossRef]
10. Krbata, M.; Eckert, M.; Majerik, J.; Barenyi, I. Wear Behaviour of High Strength Tool Steel 90MnCrV8 in Contact with Si_3N_4. *Matals* **2020**, *10*, 756. [CrossRef]
11. Moussaoui, A.; Abboudi, A.; Aissani, L.; Belgroune, A.; Cheriet, A.; Alhussein, A.; Rtimi, S. Effect of Mo addition on the mechanical and tribological properties of magnetron sputtered TiN films. *Surf. Coat. Technol.* **2023**, *470*, 129862. [CrossRef]
12. Rajput, S.S.; Upadhyay, C.; Gangopadhyay, S.; Fernandes, F. High-temperature tribological behaviour and machining performance of self-lubricant CrAlNAg coatings for dry milling operations. *Tribol. Int.* **2024**, *198*, 109824. [CrossRef]
13. Chetan; Ghosh, S.; Rao, P.V. Application of sustainable techniques in metal cutting for enhanced machinability: A review. *J. Clean. Prod.* **2015**, *100*, 17–34. [CrossRef]
14. Mayrhofer, P.H.; Clemens, H.; Fischer, F.D. Materials science-based guidelines to develop robust hard thin film materials. *Prog. Mater. Sci.* **2024**, *146*, 101323. [CrossRef]
15. Naveed, M.; Qadir, A. Effect of plasma process parameters on the wear behavior of High-Power Pulsed Magnetron Sputtering Deposited Magnetron Sputtering Deposited Aluminum Titanium Nitride coating. *Open Ceram.* **2025**, *21*, 100746. [CrossRef]
16. Netto, T.R.; Evans, A.K.; Goddard, D.T.; Cooper, J.L.; Kelly, P. Effects of sample bias on wear resistance of magnetron sputtered chromium coated zirconium alloy. *Surf. Coat. Technol.* **2025**, *498*, 131847. [CrossRef]
17. Zuo, B.; Yu, L.; Xu, J. The new nanocapsule structure and cyclic tribological properties of $Mo_2N/Ag/Si_3N_4$ nanocomposite film. *Ceram. Int.* **2023**, *49*, 38982–38994. [CrossRef]
18. Yuan, Z.; Li, Y.; Sun, L.; Yang, J.; Mei, S.; Xiong, X.; Fang, Q.; Chen, Z.; Liu, Y. Microstructures and tribological properties of MoS_2/Mo_2N multilayer gradient films deposited by reactive magnetron sputtering. *J. Mater. Res. Technol.* **2024**, *31*, 1507–1517. [CrossRef]
19. Ju, H.; Zhou, R.; Liu, S.; Yu, L.; Xu, J.; Geng, Y. Enhancement of the tribological behavior of self-lubricating nanocomposite Mo_2N/Cu films by adding the amorphous SiN_x. *Surf. Coat. Technol.* **2021**, *423*, 127565. [CrossRef]
20. Bouaouina, B.; Besnard, A.; Abaidia, S.E.; Airoudj, A.; Bensouici, F. Correlation between mechanical and microstructural properties of molybdenum nitride thin films deposited on silicon by reactive R. F. magnetron discharge. *Surf. Coat. Technol.* **2018**, *333*, 32–38. [CrossRef]
21. Liang, B.; Hsieu, F.; Wu, F. Modulation effect on mechanical properties of nanolayered MoN/MoSiN coatings. *Surf. Coat. Technol.* **2022**, *436*, 128278. [CrossRef]
22. Lin, Z.; Liu, Y.; Huang, C.; Guillon, M.; Wu, F. Input power effect on microstructure and mechanical properties of Mo-Si-N multilayer coatings. *Surf. Coat. Technol.* **2020**, *383*, 125222. [CrossRef]
23. Jiang, Y.; Wu, X.; Yu, L.; Chen, C.; Han, H.; Bian, S.; Zuo, B.; Zhao, L.; Xu, J. In-situ tribo-induced formation of superb lubricious carbon-based tribofilms on the catalytical active MoN-Ag film surfaces. *Tribol. Int.* **2024**, *196*, 109715. [CrossRef]
24. Sube, T.; Kommer, M.; Fenker, M.; Hader, B.; Albrecht, J. Reduced friction on γ-Mo $_2$ N coatings deposited by high power impulse magnetron sputtering on microstructured surfaces. *Tribol. Int.* **2017**, *106*, 41–45. [CrossRef]
25. Pappacena, K.E.; Singh, D.; Ajayi, O.O.; Routbort, J.L.; Erilymaz, O.L.; Demas, N.G.; Chen, G. Residual stresses, interfacial adhesion and tribological properties of MoN/Cu composite coatings. *Wear* **2012**, *278–279*, 62–70. [CrossRef]
26. Zhou, R.; Ju, H.; Liu, S.; Zhao, Z.; Xu, J.; Yu, L.; Qian, H.; Jia, S.; Song, R.; Shen, J. The influences of Ag content on the friction and wear properties of TiCN-Ag films. *Vacuum* **2022**, *196*, 110719. [CrossRef]
27. Aouadi, S.M.; Paudel, Y.; Simonson, W.J.; Ge, Q.; Kohli, P.; Muratore, C.; Voevodin, A.A. Tribological investigation of adaptive $Mo_2N/MoS_2/Ag$ coatings with high sulfur content. *Surf. Coat. Technol.* **2009**, *203*, 1304–1309. [CrossRef]
28. Liu, Y.; Yao, Z.; Zhang, P.; Lin, S.; He, M.; Wang, X.; Lu, S.; Wu, X. FeCrMnVSix high entropy alloy coatings with improved high temperature tribological properties via synergistic effect of in situ-formed SiO_2 and bimetallic oxides. *Tribol. Int.* **2023**, *189*, 108980. [CrossRef]
29. Gulbinski, W.; Suszko, T. Thin films of Mo_2N/Ag nanocomposite-the structure, mechanical and tribological properties. *Surf. Coat. Technol.* **2006**, *201*, 1469–1476. [CrossRef]
30. Xu, X.; Sun, J.; Su, F.; Li, Z.; Chen, Y.; Xu, Z. Microstructure and tribological performance of adaptive MoN-Ag nanocomposite coatings with various Ag contents. *Wear* **2022**, *488–489*, 204170. [CrossRef]

31. Liu, C.; Ju, H.; Yu, L.; Xu, J.; Geng, Y.; He, W.; Jiao, J. Tribological Properties of Mo_2N Films at Elevated Temperature. *Coatings* **2019**, *9*, 734. [CrossRef]
32. Mulligan, C.P.; Blanchet, T.A.; Gall, D. CrN-Ag nanocomposite coatings: High-temperature tribological response. *Wear* **2010**, *269*, 125–131. [CrossRef]
33. Chang, C.; Huang, C.; Lin, C.; Yang, F.; Tang, J. Mechanical properties of amorphous and crystalline CrN/CrAlSiN multilayer coating fabricated using HPPMS. *Surf. Interfaces* **2022**, *31*, 102064. [CrossRef]
34. Gupta, A. X-ray and neutron studies of nanoscale atomic diffusion in thin films and multilayers. *Appl. Surf. Sci.* **2009**, *256*, 552–557. [CrossRef]
35. Ni, J.; Zhao, X.; Zhao, J. P-type transparent conducting SnO_2: Zn film derived from thermal diffusion of Zn/SnO_2/Zn multilayer thin films. *Surf. Coat. Technol.* **2012**, *206*, 4356–4361. [CrossRef]
36. Hu, X.; Qiu, L.; Pan, X.; Zhang, J.; Li, X.; Zhang, S.; Dong, C. Nitrogen diffusion mechanism, microstructure and mechanical properties of thick Cr/CrN multilayer prepared by arc deposition system. *Vacuum* **2022**, *199*, 110902. [CrossRef]
37. Ju, H.; Guo, J.; Yu, L.; Xu, J.; Luan, J. Enhancement of the mechanical and tribological properties of self-lubricant Mo_2N-Ag composite film by adding amorphous SiN_x. *Ceram. Int.* **2024**, *50*, 8463–8571. [CrossRef]
38. Ju, H.; Zhou, R.; Luan, J.; Yu, L.; Xu, J.; Zuo, B.; Yang, J.; Geng, Y.; Zhao, L.; Fernandes, F. Multilayer Mo_2N-Ag/SiN_x films for demanding applications: Morphology, structure and temperature-cycling tribological properties. *Mater. Des.* **2022**, *223*, 111128. [CrossRef]
39. Ju, H.; Huang, K.; Luan, J.; Geng, Y.; Yang, J.; Xu, J. Evaluation under temperature cycling of the tribological properties of Ag-SiN_x films or green tribological applications. *Ceram. Int.* **2023**, *49*, 30115–30124. [CrossRef]
40. Janssen, G.; Abdalla, M.; Keulen, F.; Pujada, B.; Venrooy, B. Cerebrating the 100th anniversary of the Stoney equation for film stress: Developments from polycrystalline steel strips to single crystal silicon wafers. *Thin Solid Film.* **2009**, *517*, 1858. [CrossRef]
41. Kraghelsky, I.V. Calculation of Wear Rate. *J. Fluids Eng.* **1965**, *87*, 785–790. [CrossRef]
42. Xi, Y.; Gao, K.; Pang, X.; Yang, H.; Xiong, X.; Li, H.; Volinsky, A.A. Film thickness effect on texture and residual stress sign transition in sputtered TiN thin films. *Ceram. Int.* **2017**, *43*, 11992–11997. [CrossRef]
43. Ju, H.; Luan, J.; Wang, Y.; Bondarev, A.; Evaristo, M.; Geng, Y.; Xu, J.; Cavaleiro, A.; Fernandes, F. Mutual promotion on the mechanical and tribological properties of the nacre-like self-lubricant film designed for demanding green tribological applications. *Friction* **2025**, *13*, 9440963. [CrossRef]
44. Luan, J.; Kong, F.; Xu, J.; Fernandes, F.; Evaristo, M.; Dong, S.; Cavaleiro, A.; Ju, H. Deciphering the mechanical strengthening mechanism: Soft metal doping in ceramic matrices-A case study of TiN-Ag films. *Mater. Des.* **2024**, *248*, 113489. [CrossRef]
45. Chen, P.; Wang, W.; Wu, Y. Experimental investigation of thin film stress by Stoney' formula. *Measurement* **2019**, *143*, 39–50. [CrossRef]
46. Tillmann, W.; Grisales, D.; Stangier, D.; Thomann, C.; Debus, J.; Nienhaus, A.; Apel, D. Residual stresses and tribomechanical behaviour of TiAlN and TiAlCN monolayer and multilayer coatings by DCMS and HiPIMS. *Surf. Coat. Technol.* **2021**, *406*, 126664. [CrossRef]
47. Yadav, A.; Bajtošová, L.; Cieslar, M.; Fikar, J. Two-phase model for inverse Hall-Petch effect in nanocrystalline thin film: Atomistic simulation study. *Acta Mater.* **2024**, *276*, 120084. [CrossRef]
48. Dai, X.; Wen, M.; Huang, K.; Wang, X.; Yang, L.; Wang, J.; Zhang, K. Toward low friction in water for Mo_2N/Ag coatings by tailoring the wettability. *Appl. Surf. Sci.* **2018**, *447*, 886–893. [CrossRef]
49. Gulbinski, W.; Suszko, T.; Sienicki, W.; Warcholinski, B. Tribological properties of silver-and copper-doped transition metal oxide coatings. *Wear* **2003**, *254*, 129–135. [CrossRef]
50. Nicotra, G.; Spinella, C.; La Magna, A.; Bongiorno, C.; Rimini, E. Quantitative study of the Si/SiO_2 phase separation in substoichiometric silicon oxide films. *Mater. Sci. Eng. B* **2009**, *159–160*, 80–82. [CrossRef]
51. Gulbinki, W.; Suszko, T. Thin films of MoO_3-Ag_2O binary oxides-the high temperature lubricants. *Wear* **2006**, *261*, 867–873. [CrossRef]
52. Zhu, B.; Shang, L.; Bian, Y.; Li, W.; Shao, L.; Zhang, C. Enhancement mechanism of HVOF interlayers on *ta*-C film load-bearing and wear resistance. *Surf. Coat. Technol.* **2025**, *508*, 132158. [CrossRef]
53. Zhou, S.; Zhao, W.; Qiu, Z.; Lin, S.; Zheng, Z.; Zeng, D.C. Improved load-bearing capacity of Mo-doped Ti-N coatings: Effects of Mo alloying and GB plasticity. *Surf. Coat. Technol.* **2021**, *424*, 127630. [CrossRef]
54. Song, H.; Zhang, H.; Yang, S.; Nan, Y.; Mu, Y.; Chu, W.; Yang, K.; Li, H.; Pang, M.; Jiang, N.; et al. Multi-layer design for the diamond coating with anti-tribocorrosive properties under high load-bearing in simulated seawater environment. *Diam. Relat. Mater.* **2025**, *155*, 112270. [CrossRef]